J Therm Anal Calorim (2012) 107:983–987
DOI 10.1007/s10973-011-1689-0

# Decomposition processes of nickel hydroxide

**V. Logvinenko · V. Bakovets · L. Trushnikova**

Received: 9 March 2011 / Accepted: 19 May 2011 / Published online: 3 June 2011


**Abstract** The dehydration processes of nickel hydroxide were studied by means of thermogravimetry in a temperature range from 300 to 900 K. The kinetics of the low-temperature dehydroxylation ($\approx$300–600 K) was studied under non-isothermal conditions. A model-free method was used to calculate the activation energy and to analyze the stepwise checking; the non-linear regression method was applied to calculate the kinetic parameters of multi-stage decomposition reactions. The features of the dehydroxylation kinetics for the multi-stage process are explained by the formation and decomposition of hydrogel and xerogel phases.

**Keywords** Metal hydroxides · Model-free kinetics · Nano-dimensional materials · Non-isothermal kinetics · Thermal analysis

## Introduction

The dehydration of metal hydroxides is a routine process for the production of nanostructured oxide materials. The synthesis of porous microspheres, nanobelts, nanowires, nanoplates, nanosheets, and nanocolumn blocks has been described for nickel oxide materials [1–4]. The materials such as ordered mesoporous NiO with thick crystalline walls and a bimodal pore size (with 3.3 and 11 nm diameters) [5] and coralloid nanostructured NiO [6] are available now.

V. Logvinenko (✉) · V. Bakovets · L. Trushnikova
Nikolaev Institute of Inorganic Chemistry, Siberian Branch of the Russian Academy of Sciences, Ac. Lavrentyev Ave. 3, Novosibirsk, Russia 630090
e-mail: val@niic.nsc.ru

The synthesis of proper nickel hydroxide, suitable for the synthesis of the mentioned mesoporous oxide materials, is an intricate problem. The thermal decomposition of nickel hydroxide is a complex process that includes both the dehydration and dehydroxylation reactions. A study of the decomposition kinetics can help to understand the complexity of the formation of oxide nanostructured materials.

## Experimental

### Synthesis

Nickel hydroxide was prepared by the precipitation with alkali from nickel nitrate solutions (at 333 K). The precipitate was filtered off, washed with water, and dried at 323 K. The composition of the substance before the drying corresponds to the formula $Ni(OH)_2 \cdot 1.3\ H_2O$; after drying, $Ni(OH)_2 \cdot 0.45\ H_2O$ [1].

### Thermal analysis

TG measurements were carried out on a Netzsch TG 209 F1 thermal analyzer. The experiments were performed in a helium flow (80 $cm^3\ min^{-1}$) at heating rates of 5, 10, and 20 K $min^{-1}$; a corundum sample holder was used; the sample mass was kept cca 12.0–15.0 mg.

### Kinetic analysis under non-isothermal conditions

Thermogravimetric data were processed using the Netzsch Thermokinetics 2 (Version 2004.05) program [7]. A special Model Free program based on the well-known works

[8–17] allows the processing of several thermogravimetric curves obtained with different heating rates and the calculation of the activation energy without the preliminary information about the kinetic topochemical equations.

The Ozawa–Flynn–Wall Analysis program was used to calculate the activation energies for each experimental point of degree of conversion (in the range $0.005 < \alpha < 0.995$). The Ozawa–Flynn–Wall Analysis is based on the dependence between the heating rate and inverse temperature. Further, we used the same set of experimental data to search for the topochemical equation (the selection was made from 16 equations: chemical reaction at the interface, nucleation, and diffusion). This calculation is performed by the improved differential method of Borchardt–Daniels with the multiple linear regression method. It is very important that the range of the degree of conversion ($\alpha$) for this calculation can be chosen based on the relative constancy of the calculated kinetic parameters from the Ozawa–Flynn–Wall Analysis. The $F$ test is used to search for the best kinetic description (see Tables).

The $F$ test is used for the statistical control of the obtained equation. It tests the residual variances of the individual models against one another and answers the question, whether the models differ significantly (statistically speaking) or not. If $F_{\exp(1)} \approx F_{\exp(2)}$ for two equations, there is no reason to assume the first model to be better for the characterization of the experiment. The statistical quantile $F_{\text{crit}}$ is obtained for a level of significance of 0.05.

If the calculation results in two or three kinetic equations with close values of the correlation coefficients and the $F$ test, but with noticeably different values of the kinetics parameters, it is more correct to choose the equation with the activation energy values close to the data of the Model Free program. The difference between two steps was very relative in this search for topochemical equations, but it helps to find the most reliable ones.

A special nonlinear regression program is useful for the search for a full set of kinetic parameters of multi-step processes. The closest fit between the activation energies from the Model-Free analysis and the data from the nonlinear regression calculation is important from a physicochemical point of view; so the authors of the used computer program recommend to fix $E_a$ values (obtained by linear regression and congruent with $E_a$ from the Model-Free analysis) in calculations with this program.

A random error in the activation energies of such a reversible decomposition reaction in these experiments is usually about 10%, and we took this into consideration.

The NETZSCH Thermokinetics 2 computer program enables the estimation of step contributions (in $\Delta m$ percentage) after the nonlinear regression calculation.

From the standpoint of classical chemistry of solids these kinetic parameters ($E_a$, A) are not related to the elementary act; the activated complex size and configuration are unknown, so the kinetic parameters calculated for the single compound are apparent and have limited physical meaning.

However, very important is the general trend in the variation of these values within a specially selected series of compounds (either isostructural or genetically related) because the expected disorder in the reaction zones can be identical for them; all other errors will be minimized and smoothed in such a comparison [18–21]. We intend to study the thermal decomposition of several different metal hydroxides (nickel, gadolinium, and yttrium) and compare the steps of the dehydration and dehydroxylation reactions.

## Results and discussion

Metal hydroxides usually entrap a noticeable amount of water during the synthesis; it is evident from the total mass loss in thermal decomposition to metal oxide. This water starts to leave from the beginning of the heating; two stages of mass losses (dehydration and dehydroxylation) are distinguished in the DTG curve (Fig. 1). The complete decomposition process can be divided into two steps: 290–430 and 430–900 K. The completion of the thermal decomposition (595–900 K) is very prolonged (Fig. 2); this is typical of the dehydroxylation only for certain compounds.

The decomposition at 430–870 K was chosen for the kinetic study; it corresponds to the dehydroxylation: $Ni(OH)_2 \rightarrow NiO + H_2O\uparrow$ (Figs. 1 and 2).

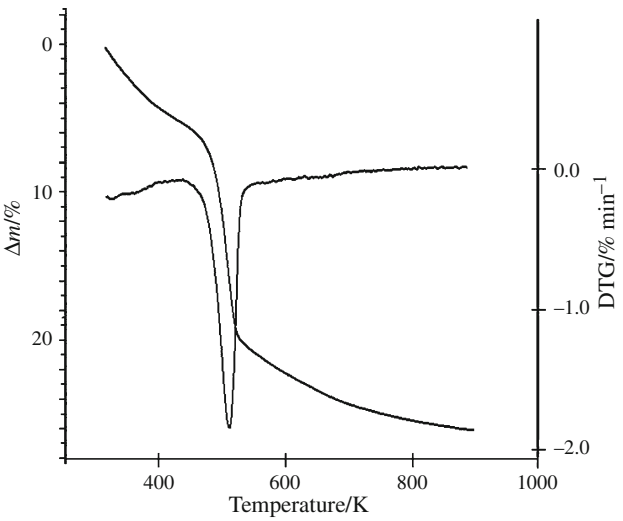


**Fig. 1** Decomposition of nickel hydroxide. Corundum sample holder; sample masses 17.5 and 19.5 mg; helium flow 80 $cm^3$ $min^{-1}$; heating rate 10 K $min^{-1}$

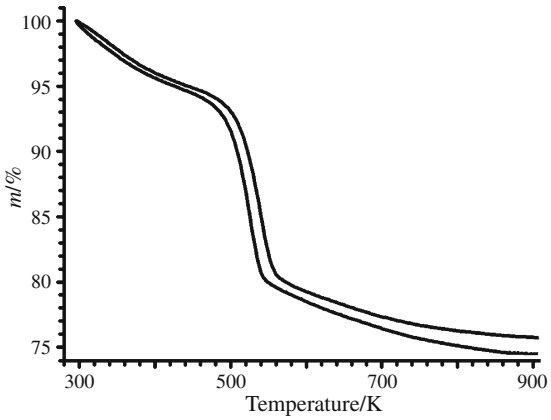


**Fig. 2** Decomposition of nickel hydroxide. Corundum sample holder; sample masses 17.5 and 19.5 mg; helium flow 80 $cm^3$ $min^{-1}$; heating rates 5 and 10 K $min^{-1}$

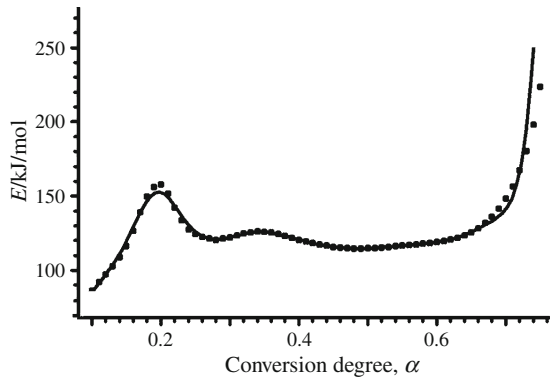


**Fig. 3** Ozawa analysis of $Ni(OH)_2$ decomposition: activation energies depending on the degree of conversion $\alpha$; the calculation was made for the whole TG curve (Fig. 2)

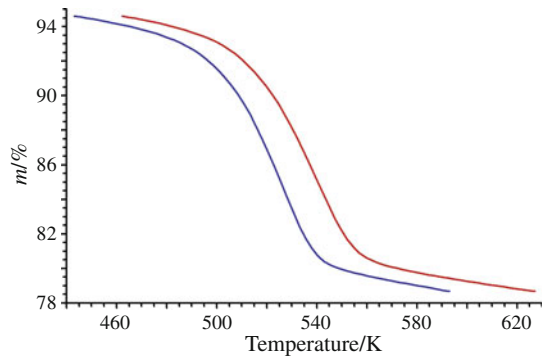


**Fig. 4** Dehydroxylation of nickel hydroxide. TG curves correspond to the narrow part of the DTG curve (see Fig. 1); heating rates 5 and 10 K $min^{-1}$

The processing of this curve by the Ozawa method (Fig. 3) shows that the activation energies, calculated beyond the degree of conversion $\alpha > 80\%$, are unconscionably and unreasonably high (>300 kJ $mol^{-1}$). The rise of the $E_a$ at $T > 590$ K seems to be caused by the steric hindrance for the complete dehydroxylation $OH^- + OH^- \rightarrow H_2O + O^{2-}$ because of a long distance between the residual $OH^-$ groups. We interpret the prolongation of the reaction time as a sharp shift of the topochemical mechanism. Therefore, only a part of the TG curve corresponding to the narrow portion DTG peak (430–595 K) was processed for the kinetic purposes (Fig. 4).

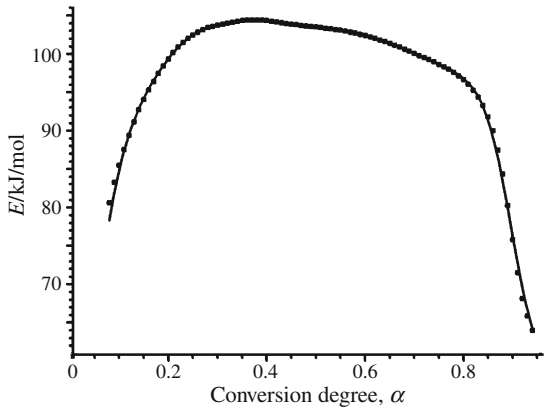


**Fig. 5** Ozawa analysis of $Ni(OH)_2$ dehydroxylation: activation energies depending on the degree of conversion $\alpha$; the calculation was made for the part of the TG curve (see Fig. 4)

The main body of the dehydroxylation (15−80% of the transformation) has a constant value of the activation energy $E_a = 100 \pm 4$ kJ $mol^{-1}$ (Fig. 5). The kinetic description of the initial decomposition part is distorted by the preliminary water elimination; the final part is distorted by the mentioned high-temperature dehydroxylation.

The preliminary calculation ($0.15 < \alpha < 0.80$) by the nonlinear regression method shows that the best equation is Fn or CnB (the contribution of the autocatalytic reaction is insignificant):

$$f(\alpha) = (1-\alpha)^{0.71}\,(1 + 0.5\alpha),\ E_a = 101.0 \pm 1.4,$$
$$\lg A = 7.5 \pm 0.1,\ \text{Corr. coeff.} = 0.999810;$$
$$f(\alpha) = (1-\alpha)^{0.70},\ E_a = 101.0 \pm 1.3,$$
$$\lg A = 7.5 \pm 0.1,\ \text{Corr. coeff.} = 0.999797.$$

In continuation of the data analysis, three sets of equations for the description of the three-stage decomposition (A → B→C → D) were checked for the calculation by the nonlinear regression method:

(1) Fn, Fn, Fn.
(2) CnB, CnC, Fn.
(3) An, Fn, Fn.

The results of the nonlinear regression method (Table 1).

All three variants are not sufficiently distinguishable. The most probable estimate (Fig. 6):

**Table 1** Results of the kinetic analysis of the dehydroxylation

| Equations/$f(\alpha)$ | $F_{crit}$ | $F_{exp}$ | $E_a$/kJ/mol$^{-1}$ | lg A | Reaction contribution/% | Corr. coeff |
|---|---|---|---|---|---|---|
| (I) $(1-\alpha)^{2.9}$ | | | 74 | 5.9 | 9.1 | |
| (II) $(1-\alpha)^{0.58}$ | 1.38 | 1.00 | 113 | 8.9 | 51.9 | 0.999995 |
| (III) $(1-\alpha)^{0.47}$ | | | 100 | 7.5 | 29.0 | |
| (I) $(1-\alpha)^{3.0}(1+0.0001\alpha)$ | | | 75 | 6.0 | 8.6 | |
| (II) $(1-\alpha)^{0.58}(1+0.0001\alpha)$ | 1.38 | 1.01 | 107 | 8.3 | 79.2 | 0.999995 |
| (III) $(1-\alpha)^{2.56}$ | | | 181 | 16.1 | 12.2 | |
| (I) $(1-\alpha)[-\ln(1-\alpha)]^{1.15}$ | | | 78 | 6.8 | 3.1 | |
| (II) $(1-\alpha)^{3.4}$ | 1.38 | 1.68 | 78 | 6.4 | 4.5 | 0.999992 |
| (III) $(1-\alpha)^{0.59}$ | | | 111 | 8.7 | 92.4 | |

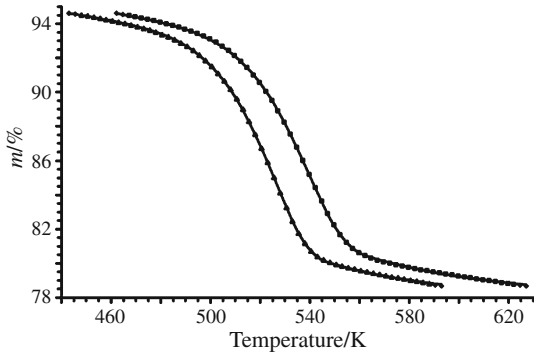


**Fig. 6** Data processing for $Ni(OH)_2$ dehydroxylation. TG curves (5 and 10 K min$^{-1}$) fitting of non-linear regression, simulated with Fn equations for all three steps. Experimental points, calculated lines

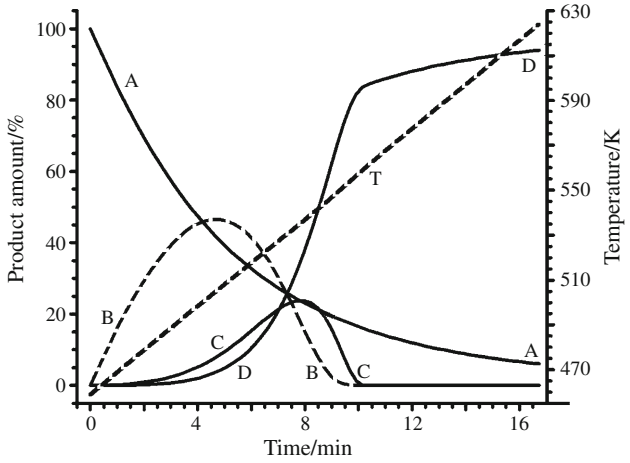


**Fig. 7** Decomposition of nickel hydroxide. Time dependence of the yield for each reactant in the dehydroxylation. The calculation corresponds to the three-stage process (A → B → C → D) in Fig. 6

$$f(\alpha)_1 = (1-\alpha)^{2.9},\ E_1 = 74 \pm 4 \text{ kJ mol}^{-1},\ \text{lgA} = 5.9 \pm 0.5;$$

$$f(\alpha)_2 = (1-\alpha)^{0.58},\ E_2 = 114 \pm 1 \text{ kJ mol}^{-1},\ \text{lgA} = 8.9 \pm 0.1;$$

$$f(\alpha)_3 = (1-\alpha)^{0.47},\ E_3 = 100 \pm 1 \text{ kJ mol}^{-1},\ \text{lgA} = 7.5 \pm 0.1;\ \text{Corr. coeff.} = 0.999995.$$

The time dependences of the yield for each reactant in the dehydroxylation are shown in Fig. 7.

The step A → B (9.1% of the mass loss) can be related to the breakdown of the residual hydrogel and its dehydration (430–630 K); a high order of the equation ($n = 2.9$) can be due to a particle size increase at 500–600 K [1].

The main part of the decomposition, B → C → D (the second and third stages, 61.9% + 29.0% = 90.9%) is described by the equations of the chemical reaction at the interface (the contracting sphere and the cylinder; the reaction order changes from $n = 0.58$ to 0.47). The activation energy is first similar to the value calculated by the Model-Free method (Fig. 5, $0.15 < \alpha < 0.80$) and then decreases.

Air-dried nickel hydroxide contains the hydrate water $Ni(OH)_2 \cdot 1.3\ H_2O$. The existence of water molecules in synthesized nickel hydroxide can be explained by the intercalation of a water layer inside the α-$Ni(OH)_2$ structure [22].

The dehydrated substance with the stoichiometric composition $Ni(OH)_2$, obtained after the isothermal dehydration at 500 K, in fact, can be attributed to two-phase xerogel ($NiO + Ni(OH)_2 \cdot H_2O$) [1].

## Conclusions

A quantitative description of the decomposition kinetics for nickel hydroxide is not simple. The step-by-step complexity can be explained by the probable occurrence of the intercalation of a water layer inside the α-$Ni(OH)_2$ structure [22] and two-phase xerogel {$NiO + Ni(OH)_2$} [1] and can be associated with the dehydration and dehydroxylation.

The observed incomplete dehydroxylation of nickel hydroxide until 900 K (Fig. 1) must be due to the features of the topochemistry of the decomposition. One possible explanation is the retention of hydroxyls inside the structure of nickel oxide grains. The steric hindrance for the completion of the dehydroxylation $OH^- + OH^- \rightarrow O^{2-} + H_2O\uparrow$ (because of a long distance between the rare residual $OH^-$ groups) becomes evident from the unreasonably high (calculated) activation energy (>300 kJ $mol^{-1}$) at $T > 590$ K (Fig. 3).

The decomposition process at these temperatures can be related to the loss of the water molecules, product of dehydroxylation process, which has been trapped in the framework of the dehydroxylated product (e.g., [23, 24]).

## References


1. Bakovets VV, Trushnikova LN, Korol'kov IV, Sokolov VV, Dolgovesova IP, Pivovarova TD. Synthesis of nanostructured nickel oxide. Russ J Gen Chem. 2009;79:356–61.
2. Dong L, Chu Y, Sun W. Controllable synthesis of nickel hydroxide and porous nickel oxide nanostructures with different morphologies. Chem A Europ J. 2008;14:5064–72.
3. Kuang D-B, Lei B-X, Pan Y-P, Yu X-Y, Su C-Y. Fabrication of novel hierarchical $\beta$-$Ni(OH)_2$ and NiO microspheres via an easy hydrothermal process. J Phys Chem C. 2009;113:5508–13.
4. Zhu J, Gui Z, Ding Y, Wang Z, Hu Y, Zou M. A facile route to oriented nickel hydroxide nanocolumns and porous nickel oxide. J Phys Chem C. 2007;111:5622–7.
5. Jiao F, Hill AH, Harrison A, Berko A, Chadwick AV, Bruce PG. Synthesis of ordered mesoporous NiO with crystalline walls and a bimodal pore size distribution. J Amer Chem Soc. 2008;130:5262–6.
6. Lai T-L, Lai Y-L, Yu J-W, Shu Y-Y, Wang C-B. Microwave-assisted hydrothermal synthesis of coralloid nanostructured nickel hydroxide hydrate and thermal conversion to nickel oxide. Mater Res Bull. 2009;44:2040–4.
7. Netzsch Thermokinetics 2. Version 2004.05. http://www.therm-soft.com.
8. Kissinger HE. Reaction kinetics in differential thermal analysis. Anal Chem. 1957;29:1702–6.
9. Friedman HL. Kinetics of thermal degradation of char-forming plastics from thermogravimetry. J Polym Sci (C). 1963;6:183–95.
10. Ozawa T. A new method of analyzing thermogravimetric data. Bull Chem Soc Japan. 1965;38:1881–6.
11. Ozawa T. Estimation of activation energy by isoconversion methods. Thermochim Acta. 1992;203(C):159–65.
12. Flynn JH, Wall LA. General treatment of the thermogravimetry of polymers. J Res Nat Bur Stand. 1966;70:478–523.
13. Opfermann J, Kaisersberger E. An advantageous variant of the Ozawa–Flynn–Wall analysis. Thermochim Acta. 1992;203(C):167–75.
14. Opfermann JR, Kaisersberger E, Flammersheim HJ. Model-free analysis of thermo-analytical data-advantages and limitations. Thermochim Acta. 2002;391:119–27.
15. Vyazovkin S. Model-free kinetics: staying free of multiplaying entities without necessity. J Therm Anal Calorim. 2006;83:45–51.
16. Simon P. The single-step approximation: attributes, strong and weak sides. J Therm Anal Calorim. 2007;88:709–15.
17. Simon P. Single-step kinetics approximation employing non-arrhenius temperature functions. J Therm Anal Calorim. 2005;79:703–8.
18. Logvinenko V. Stability and reactivity of coordination and inclusion compounds in the reversible processes of thermal dissociation. Thermochim Acta. 1999;340–1:293–9.
19. Logvinenko V. Solid state coordination chemistry. The quantitative thermoanalytical study of thermal dissociation reactions. J Therm Anal Calorim. 2000;60:9–15.
20. Logvinenko V, Fedorov V, Mironov Yu, Drebushchak V. Kinetic and thermodynamic stability of cluster compounds under heating. J Therm Anal. 2007;88:687–92.
21. Logvinenko V, Drebushchak V, Pinakov D, Chekhova G. Thermodynamic and kinetic stability of inclusion compounds under heating. J Therm Anal. 2007;90:23–30.
22. Freitas MBJG, Silva RKS, Anjos DM, Rozario A, Manoel PG. Effect of synthesis conditions on characteristics of the precursor material used in $NiO{\cdot}OH/Ni(OH)_2$ electrodes of alkaline batteries. J Power Sources. 2007;165:916–21.
23. Franco F, Ruiz Cruz MD. A comparative study of the dehydroxylation process in untreated and hydrazine–deintercalated dickite. J Therm Anal Calorim. 2006;85:369–75.
24. Vergbitsky FR. High-frequency thermal analysis, 2nd edn. Perm: Perm State University; 1981 (in Russian).